Energy & Environmental Science

Cite this: *Energy Environ. Sci.*, 2011, **4**, 3980

www.rsc.org/ees

COMMUNICATION

# High surface area, micro/mesoporous carbon particles with selectable 3-D biogenic morphologies for tailored catalysis, filtration, or adsorption†

**Zhihao Bao,‡[a] Min-Kyu Song,‡[b] Stanley C. Davis,[b] Ye Cai,[b] Meilin Liu[b] and Kenneth H. Sandhage*[b]**

***Received 8th July 2011, Accepted 25th August 2011***
**DOI: 10.1039/c1ee02102h**



**Biogenic 3-D $SiO_2$ micro-assemblies (diatom microshells) of low specific surface area (SSA, <2 $m^2g^{-1}$) have been transformed into 3-D replicas of high SSA C (>1300 $m^2g^{-1}$) and Pt-loaded C (>600 $m^2g^{-1}$) by a shape-preserving serial reaction process. Such high SSA micro-assemblies may be generated in a wide variety of selectable 3-D shapes for tailored catalysis, filtration, or adsorption for energy storage/production, water purification, and biofuel separation.**

Highly-porous carbon assemblies have attracted appreciable interest as catalyst supports in fuel cells or sensors, as electrodes for supercapacitors or batteries, and as adsorbants for hydrogen or natural gas storage, carbon dioxide capture, and (bio)chemical or water purification.[1] Templating approaches have been used to generate very high surface area (>1,000 $m^2g^{-1}$) porous carbon structures with simple shapes (*e.g.*, spheres, tubes, films) or with complex but uncontrolled irregular shapes (*e.g.*, non-uniform powders).[2] Here we demonstrate a shape-preserving serial reaction process for converting complex-shaped, three-dimensional (3-D) biogenic $SiO_2$ micro-assemblies (*i.e.*, the microshells, or frustules, of single-celled aquatic algae known as diatoms) of low specific surface area (SSA <2 $m^2g^{-1}$) into positive 3-D replicas comprised of micro/mesoporous C of very high SSA (>1,300 $m^2g^{-1}$). To our knowledge, this is the first report of a method capable of yielding such high-SSA carbon assemblies in a wide variety of complex 3-D microscale morphologies available from biogenic[3] or synthetic[4] templates (*e.g.*, each of the tens of thousands of extant diatom species forms a silica frustule with a unique 3-D morphology[3b]). While diatom frustules have been used as passive (non-reacting) scaffolds for the infiltration of C-bearing precursors (sucrose, furfuryl alcohol[5]), subsequent carbonization heat treatment and $SiO_2$ dissolution has yielded negative C replicas with much lower values of SSA (169–312 $m^2g^{-1}$) than observed for the reaction-induced positive replicas of the present work. The ability to synthesize microscale high-SSA carbon assemblies with selectable 3-D morphologies can provide for enhanced control of adsorption, filtration, or catalysis. Indeed, upon loading with Pt nanoparticles, the 3-D high-SSA C frustule replicas of the present work exhibited significantly higher electrocatalytic activity for oxygen reduction (under conditions relevant for polymer electrolyte fuel cells) than irregular particles of Pt-bearing commercial C black and SiC-derived C of comparable SSA.

[a]*Shanghai Key Laboratory of Special Artificial Microstructure Materials and Technology, Tongji University, Shanghai, 200092, P. R. China*
[b]*School of Materials Science and Engineering, Georgia Institute of Technology, 771 Ferst Drive, Atlanta, GA 30332-0245, U.S.A. E-mail: ken.sandhage@mse.gatech.edu; Fax: (+1) 404 385 3734; Tel: (+1) 404 894 6882*

† Electronic supplementary information (ESI) available: Experimental details on the syntheses and characterization of C replicas, along with Figures S1–S3. See DOI: 10.1039/c1ee02102h

‡ These authors contributed equally to this work.

## Broader context

The electrical, chemical, and mechanical characteristics of carbon have made this material attractive for energy storage/harvesting, environmental remediation, and (bio)chemical separation (*e.g.*, as electrodes for batteries or supercapacitors; catalyst supports in fuel cells or sensors; adsorbants for hydrogen or natural gas storage, carbon sequestration, water purification, and biofuel separation). The performance of carbon is strongly dependent upon the carbon morphology, specific surface area (SSA), and pore size distribution. To date, high SSA (>1,000 $m^2g^{-1}$) carbon has been produced in simple regular shapes (spheres, tubes, films) or uncontrolled irregular shapes (non-uniform powders). Herein, we demonstrate, for the first time, a bio-enabled process for synthesizing micro/mesoporous carbon of very high SSA (>1,300 $m^2g^{-1}$) *and* with complex, but controlled three-dimensional (3-D) morphologies inherited from the silica microshells of diatoms (unicellular algae). The low SSA (<2 $m^2g^{-1}$) silica microshells are transformed into 3-D carbon replicas of very high SSA (>1,300 $m^2g^{-1}$) by a series of shape-preserving reactions. Upon loading with Pt nanoparticles, the 3-D high-SSA C microshell replicas exhibited significantly higher oxygen reduction activity (*e.g.*, for fuel cells) than irregular Pt-bearing C particles of comparable SSA. High-SSA carbon assemblies with a wide range of 3-D architectures selected from biogenic silica templates may be generated for tailored catalysis, filtration, intercalation, or adsorption in environmental or energy-related applications.

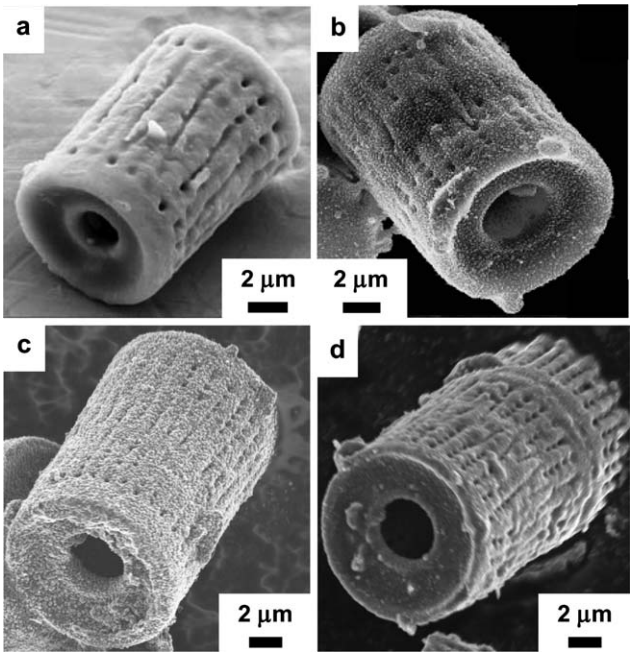


**Fig. 1** Secondary electron images of: a) a starting $SiO_2$ *Aulacoseira* diatom frustule, b) a Si replica, c) a SiC replica, and d) a C replica.

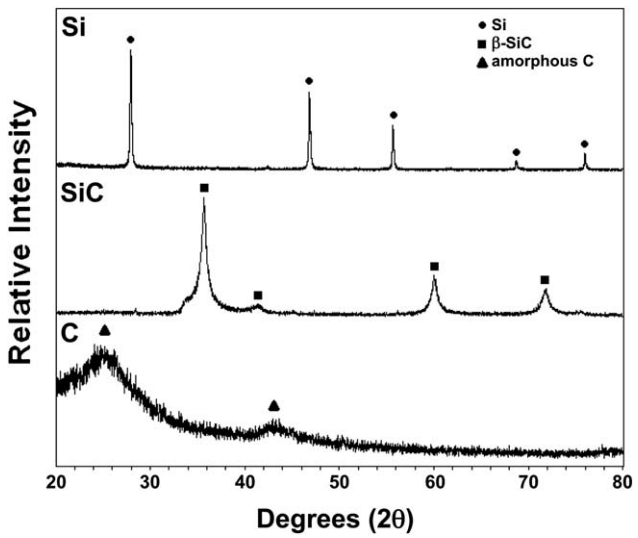


**Fig. 2** XRD patterns obtained from Si, SiC, and C replicas of *Aulacoseira* diatom frustules.

A series of shape-preserving chemical reactions was used to convert 3-D microscale silica diatom frustules of low SSA into positive 3-D carbon replicas of very high SSA for subsequent platinum loading. The starting *Aulacoseira* diatom frustules (Fig. 1a) possessed a hollow cylindrical shape, side walls with fine channels and rows of macropores ($10^2$ nm dia.), and end faces with a protruding rim and a circular hole. Nitrogen adsorption analyses indicated that these $SiO_2$ frustules possessed a SSA of only 1.65 $m^2g^{-1}$, a specific mesopore volume of <0.005 $cm^3g^{-1}$, and no detectable microporosity. The following magnesiothermic reaction[6] was used to convert *Aulacoseira* frustules into MgO/Si replicas:

$$2Mg(g) + SiO_2(s) \Rightarrow 2MgO(s) + Si(s) \quad (1)$$

The magnesia product of this reaction was removed by selective acid dissolution to yield polycrystalline silicon, as confirmed by X-ray diffraction (XRD) analysis (Fig. 2). Exposure of these porous silicon replicas to flowing methane at 950 °C for 2.5 h, followed by thermal treatment at 1200 °C for 12 h in flowing argon, resulted in conversion of the silicon into silicon carbide (β-SiC), as revealed by XRD, transmission electron microscopy (TEM), and selected area electron diffraction (SAED) analyses (Fig. 2, S1a†). The SiC structures were then exposed to $Cl_2$ gas at 950 °C for 2 h to allow for selective Si removal[7] and amorphous carbon formation, as confirmed by XRD,[8] TEM/SAED, and energy-dispersive X-ray (EDX) analyses (Fig. 2, S1b†). The C replicas were then impregnated with Pt nanoparticles *via* use of platinum dicarbonyl chloride ($Pt(CO)_2Cl_2$) vapor (230 °C, 0.5 h).[9] EDX and HRTEM analyses (Fig. 3a, 3b, S1c†) confirmed the presence of Pt nanoparticles within the porous walls of the C replicas. Thermogravimetric analysis (Fig. S2a†) indicated that the Pt-bearing C frustule replicas contained 38.3 wt% platinum.

The 3-D cylindrical morphology and fine features (rows of fine pores and channels) of the starting $SiO_2$ *Aulacoseira* frustules were retained upon reactive conversion into Si, β-SiC, and amorphous C (Fig. 1b–d). However, the porosity within the walls of these frustules replicas was altered by the reaction-induced changes in solid volume.

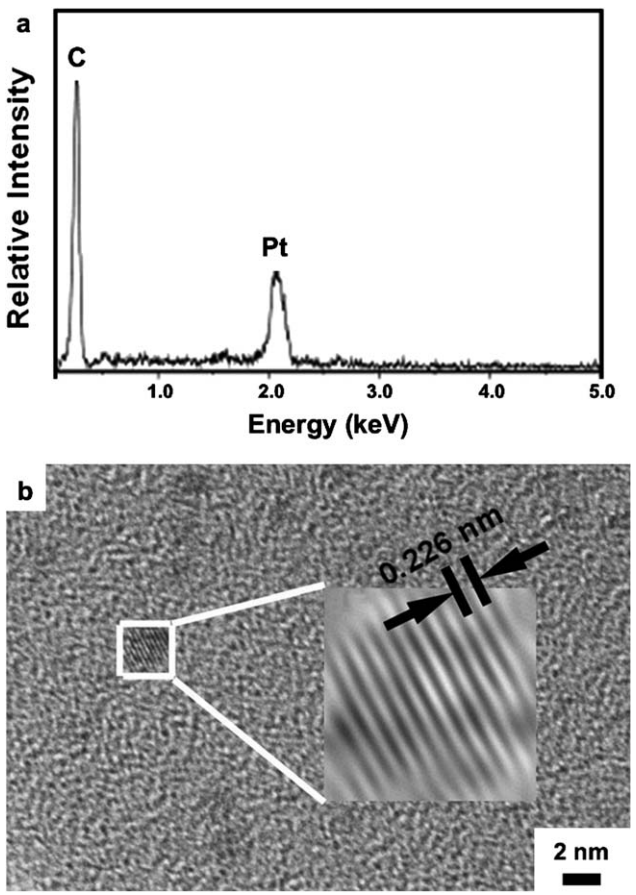


**Fig. 3** a) EDX analysis of a Pt-bearing C frustule replica, and b) HRTEM image of a cross-section of a Pt-bearing C frustule replica. The inset reveals a lattice fringe image of a fine Pt nanoparticle (note: (111) planes of platinum possess a 0.226 nm spacing).

Selective dissolution of the MgO product of reaction (1) yielded a porous, but interconnected Si network with enhanced SSA (52.6 $m^2g^{-1}$) and mesopore volume (0.448 $cm^3g^{-1}$) relative to the starting frustules. Subsequent conversion of the porous Si into β-SiC resulted in modest reductions in SSA and mesopore volume (to 48.4 $m^2g^{-1}$ and 0.370 $cm^3g^{-1}$, respectively), which was consistent with the modest difference in the volumes of Si (12.05 $cm^3mol^{-1}$) and β-SiC (12.47 $cm^3mol^{-1}$).[10] However, amorphous C possesses a significantly smaller molar volume (~5.2–6.0 $cm^3mol^{-1}$) than β-SiC.[11] Hence, since the $Cl_2$-induced selective removal of Si from the β-SiC frustules replicas yielded amorphous C replicas of similar size (*i.e.*, the β-SiC and C frustule replicas possessed diameters of ~10–11 μm, see Fig. 1C, 1D, and 5), the large reduction in solid volume associated with the conversion of β-SiC into C was accommodated by dramatic enhancements in the values of SSA (1370 $m^2g^{-1}$), mesopore volume (1.53 $cm^3g^{-1}$), and micropore volume (0.282 $cm^3g^{-1}$) for the C frustule replicas (Table 1).

In order to evaluate the utility of these hollow 3-D high-SSA carbon frustule replicas as catalyst templates, the replicas (referred to herein as $C_F$ microparticles) were impregnated with platinum nanoparticles. These Pt-bearing $C_F$ ($Pt/C_F$) microparticles possessed a SSA of 662 $m^2g^{-1}$, along with appreciable retained mesoporosity (0.689 $cm^3g^{-1}$) and reduced microporosity (0.0584 $cm^3g^{-1}$) relative to the $C_F$ microparticles (Table 1). For comparison of catalytic activity, two other types of carbon microparticles were impregnated with platinum: i) porous SiC-derived C (referred to as $C_S$ microparticles) generated *via* exposure of β-SiC powder (8.7 μm ave. dia.) to $Cl_2$(g) at 950 °C for 2 h, and ii) C black (4.9 μm ave. dia., Vulcan XC-72R, referred to as $C_V$ microparticles). The $C_S$ microparticles (Fig. S3a†) were selected for comparison to the $C_F$ microparticles, as both types of microparticles possessed similar specific values of surface area, mesopore volume, and micropore volume (*i.e.*, these values agreed to within 11%, Table 1) and comparable particle diameters (~8.7 *vs.* ~10–11 μm). Although the corresponding values of specific surface area, specific micropore volume, and specific mesopore volume for the $C_V$ powder (Fig. S3b†) were much smaller, the selection of these $C_V$ microparticles was based on the common use of this catalyst support in PEM fuel cells.[12] After Pt deposition with $Pt(CO)_2Cl_2$ vapor (230 °C, 0.5 h), the Pt-bearing $C_S$ ($Pt/C_S$) and $C_V$ ($Pt/C_V$) microparticles possessed 41.4 wt% and 14.2 wt% Pt, respectively (Figs. S2b, S2c†). That is, after Pt deposition with $Pt(CO)_2Cl_2$ vapor under identical conditions, a similar amount of Pt (38.3 and 41.4 wt %) was deposited onto $C_F$ and $C_S$ microparticles (which possessed similarly high values of SSA), whereas less Pt (14.2 wt%) was deposited onto the modest SSA $C_V$ microparticles. The resulting $Pt/C_F$ and $Pt/C_S$ microparticles also possessed higher specific values of surface area, mesopore volume, and micropore volume than did the $C/Pt_V$ microparticles (Table 1). Comparison of the micropore volumes before and after Pt deposition indicated a larger reduction in micropore volume for $C_F$ microparticles (from 0.282 to 0.0584 $cm^3g^{-1}$ = 79% reduction) than for $C_S$ (from 0.286 to 0.170 $cm^3g^{-1}$ = 41% reduction) or $C_V$ (from 0.0232 to 0.0215 $cm^3g^{-1}$ = 7.3% reduction) microparticles, which was consistent with a relatively high population of very fine (≤2 nm) Pt nanoparticles in the $Pt/C_F$ specimens (Fig. 3b).

The electrocatalytic activities of $Pt/C_F$, $Pt/C_S$, and $Pt/C_V$ microparticles for the oxygen reduction reaction (ORR) in an oxygen-saturate 0.5 M $H_2SO_4$ solution were evaluated *via* the rotating disk electrode (RDE) method. A suspension of each type of platinum-bearing microparticle in a perfluorosulfonic acid-bearing (Nafion®) solution was deposited onto a glassy carbon working electrode and dried. The microparticle content deposited onto the working electrode was adjusted to achieve a similar amount of total platinum loading (0.1 $mgcm^{-2}$) for each type of microparticle. Polarization curves are shown in Fig. 4a. At potentials ≥0.9 V (where the overall ORR rate was dominated by charge-transfer kinetics), the $Pt/C_F$-bearing working electrode exhibited substantially greater catalytic activity (carried a higher current density) than for the $Pt/C_S$-bearing or $Pt/C_V$-bearing working electrodes. Over the potential range of 0.90 to 1.05 V, the ORR activity of the $Pt/C_F$-bearing electrode (as revealed by the current density) was higher than for the $Pt/C_S$-bearing and $Pt/C_V$-bearing electrodes by factors of 4.5–4.9 and 7.7–9.2, respectively. Electrochemical impedance spectroscopic (EIS) analyses obtained at 0.8 V (*i.e.*, comparable to operating voltages used for PEM fuel cells[13]) are shown in Fig. 4b. While similar values of Ohmic resistance (given by the high frequency intercepts of the curves in Fig. 4b with the real axis) were seen for the various Pt/C-bearing electrodes, the value of interfacial charge transfer resistance (given by the difference between the high frequency and low frequency intercepts of these curves with the real axis) was appreciably lower for the $Pt/C_F$-bearing electrode than for the $Pt/C_S$-bearing and $Pt/C_V$-bearing electrodes. Chronoamperometric analysis (Fig. 4c) at 0.8 V indicated that the steady-state current for the $Pt/C_F$-bearing electrode was also significantly higher than for the $Pt/C_S$-bearing and $Pt/C_V$-bearing electrodes. It is worth noting that, although the $Pt/C_S$ microparticles possessed higher specific micropore and mesopore volumes than did the $Pt/C_F$ microparticles (Table 1), the latter microparticles exhibited significantly higher catalytic activity for ORR.

The significantly enhanced electrocatalytic activity of the $Pt/C_F$ microparticles was consistent with the presence of a higher population of very fine (≤2 nm) Pt nanoparticles (as discussed above), and a reduced oxygen diffusion distance, for these microparticles than for the $Pt/C_S$ and $Pt/C_V$ microparticles. Because the $Pt/C_F$ microparticles retained the hollow morphology of the diatom frustules, the average oxygen diffusion distance through these porous microparticles was ~0.7 μm (half the wall thickness shown in Fig. 5a and 5b), as opposed to ~4.3 μm and ~2.5 μm (half the average particle diameters) for $Pt/C_S$ and $Pt/C_V$ microparticles, respectively. The hollow and thin-walled nature of the $C_F$ microparticles, coupled with the relatively high specific micropore volume of these particles, also appears to have enabled the deposition of a relatively high population of fine platinum nanoparticles within the $C_F$ micropores. Although the $C_F$ and $C_S$ microparticles possessed similar starting

**Table 1** Specific Surface Area (SSA), Specific Micropore Volume (SMiV), and Specific Mesopore Volume (SMeV)

| Specimen[a] | SSA ($m^2g^{-1}$) | SMiV ($cm^3g^{-1}$) | SMeV ($cm^3g^{-1}$) |
|---|---|---|---|
| $C_F$ | 1370 | 0.282 | 1.53 |
| $C_S$ | 1230 | 0.286 | 1.40 |
| $C_V$ | 227 | 0.0232 | 0.413 |
| $Pt/C_F$ | 662 | 0.0584 | 0.689 |
| $Pt/C_S$ | 734 | 0.170 | 0.837 |
| $Pt/C_V$ | 141 | 0.0215 | 0.183 |

[a] $C_F$ = C frustule replicas, $C_S$ = C replicas of SiC powder; $C_V$ = C black (Vulcan XC-72R); $Pt/C_F$ = Pt-bearing C frustule replicas; $Pt/C_S$ = Pt-bearing SiC powder replicas; $Pt/C_V$ = Pt-bearing C black.

 

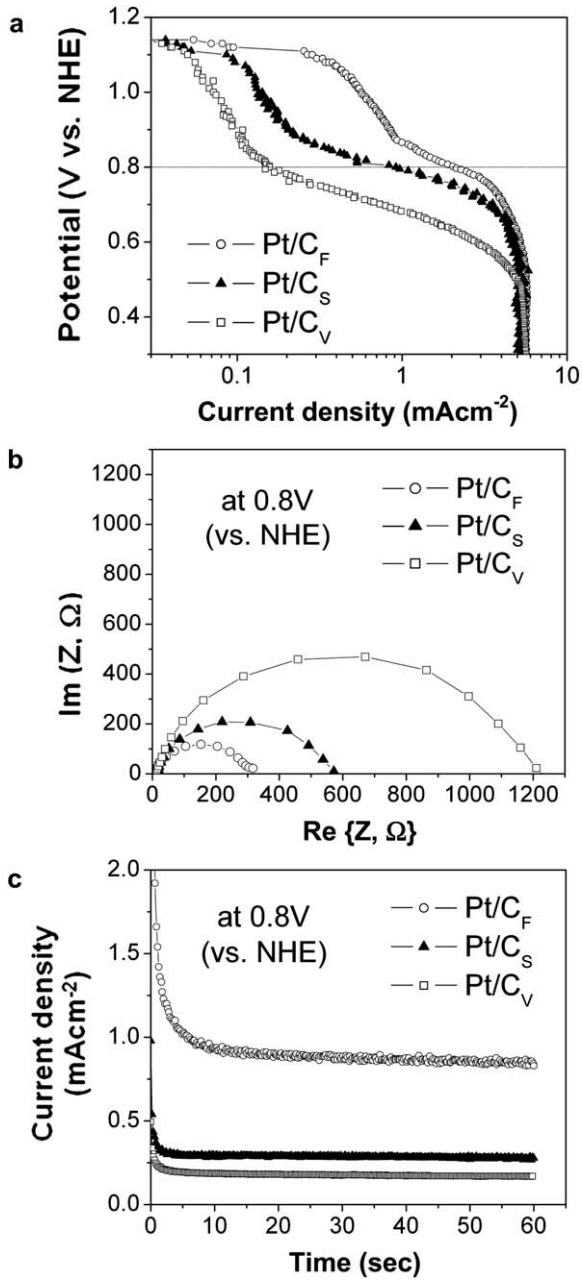


**Fig. 4** a) Polarization curves for ORR measured on a RDE in an $O_2$-saturated 0.5M $H_2SO_4$ solution at 2000 rpm with a voltage scan rate of 10 $mVsec^{-1}$, b) impedance spectra at 0.8 V under the influence of an ac voltage of 10 mV, and c) chronoamperometric curves for ORR at 0.8 V.

specific micropore volumes (0.282 and 0.286 $cm^3g^{-1}$, respectively), the shorter diffusion distance for the $C_F$ microparticles appears to have resulted in greater filling of the micropores, and the generation of a larger population of fine platinum nanoparticles, than for the $C_S$ microparticles (as indicated by the larger reduction in specific micropore volume after Pt deposition for the $C_F$ microparticles than for the $C_S$ microparticles). The relatively low population of micropores in the $C_V$ microparticles, and the small reduction in the specific micropore volume upon Pt loading of these microparticles, indicated that the population of fine Pt nanoparticles in these microparticles was low compared to the $C_F$ or $C_S$ microparticles.

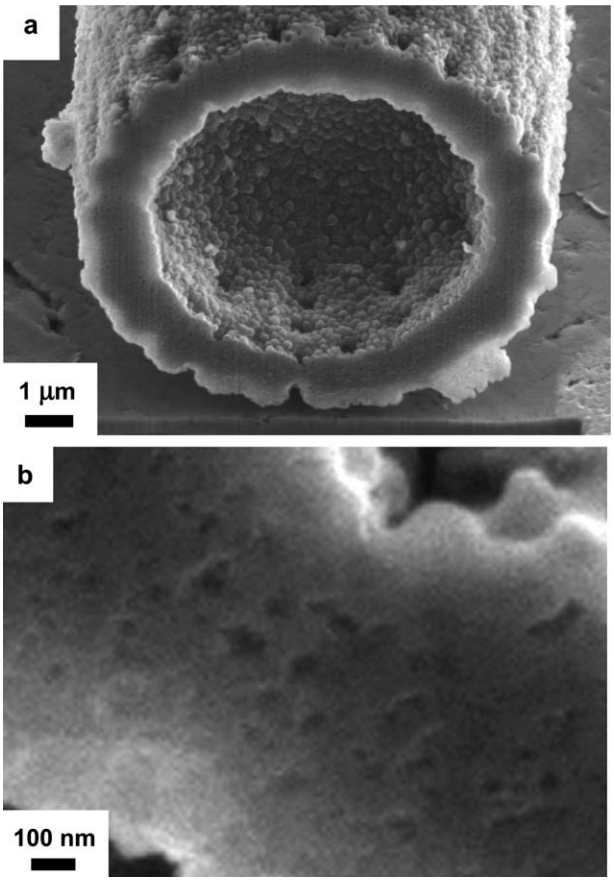


**Fig. 5** Secondary electron images of an ion-milled cross-section of a carbon replica of an *Aulacoseira* diatom frustule.

This work provides the first demonstration of the use of a series of shape-preserving reactions to transform silica templates of complex 3-D micro/nanostructured morphology and modest SSA (<2 $m^2g^{-1}$) into positive 3-D replicas comprised of micro/mesoporous carbon with very high SSA (*i.e.*, >1,300 $m^2g^{-1}$, comparable to commercial activated carbons). By allowing for the retention of the 3-D micro-scale shape and fine features of silica templates, this process enables the syntheses of high-SSA carbon assemblies with a wide variety of selectable architectures directly inherited from numerous available sustainable (inexpensive) biogenic silica[3] (as well as synthetic silica[4]) templates. Such control over 3-D morphology allows for the tailoring of fluid (gas or liquid) transport through, and nanoparticle dispersions within, highly porous carbon structures for enhanced catalysis, filtration, intercalation, or adsorption for numerous applications, such as in energy storage and harvesting, sensing, water purification, carbon sequestration, and (bio)chemical separation.[1]

## Acknowledgements

The work of MKS, SD, ML, and KHS was supported by the U.S. Department of Energy, Office of Basic Energy Sciences, Awards No. DE-SC0002245 and No. DE-SC0001061. The work of ZB and YC was supported by the U.S. Air Force Office of Scientific Research, Awards No. FA9550-05-1-0092 and No. FA9550-09-1-0162. The authors acknowledge the Georgia Tech FIB2 Center established under NSF funding.

## References


1 (*a*) M. B. Shiflett and H. C. Foley, *Science*, 1999, **285**, 1902; (*b*) S. H. Joo, S. J. Choi, I. Oh, J. Kwak, Z. Liu, O. Terasaki and R. Ryoo, *Nature*, 2001, **412**, 169; (*c*) D. Lee, J. Lee, J. Kim, J. Kim, H. B. Na, B. Kim, C.-H. Shin, J. H. Kwak, A. Dohnalkova, J. W. Grate, T. Hyeon and H.-S. Kim, *Adv. Mater.*, 2005, **17**, 2828; (*d*) J. Lee, S. Yoon, S. M. Oh, C.-H. Shin and T. Hyeon, *Adv. Mater.*, 2000, **12**, 359; (*e*) S. Wei, H. Zhang, Y. Huang, W. Wang, Y. Xia and Z. Yu, *Energy Environ. Sci.*, 2011, **4**, 736; (*f*) H. Zhao, S. Zhu, M. Hibino, I. Honma and M. Ichihara, *Adv. Mater.*, 2003, **15**, 2107; (*g*) H. Wang, Q. Gao and J. Hu, *J. Am. Chem. Soc.*, 2009, **131**, 7016; (*h*) G.-P. Hao, W.-C. Li, D. Qian and A.-H. Lu, *Adv. Mater.*, 2010, **22**, 853.

2 (*a*) C. Liang, Z. Li and S. Dai, *Angew. Chem., Int. Ed.*, 2008, **47**, 3696; (*b*) J. Lee, J. Kim and T. Hyeon, *Adv. Mater.*, 2006, **18**, 2073; (*c*) Y. Xia and R. Mokaya, *Adv. Mater.*, 2004, **16**, 886; (*d*) S. Che, A. E. Garcia-Bennett, X. Liu, R. P. Hodgkins, P. Wright, D. Zhao, O. Terasaki and T. Tatsumi, *Angew. Chem., Int. Ed.*, 2003, **42**, 3930; (*e*) J. Pang, X. Li, D. Wang, Z. Wu, V. T. John, Z. Yang and Y. Lu, *Adv. Mater.*, 2004, **16**, 884.

3 (*a*) T. L. Simpson and B. E. Volcani, *Silicon and Siliceous Structures in Biological Systems*, Springer, New York, 1981; (*b*) F. E. Round, R. M. Crawford and D. G. Mann, *The Diatoms: Biology and Morphology of the Genera*, Cambridge Univ. Press, New York, 2000.

4 (*a*) H. Yang, N. Coombs and G. A. Ozin, *Nature*, 1997, **386**, 692; (*b*) H. Fan, Y. Lu, A. Stump, S. T. Reed, T. Baer, R. Schunk, V. Perez-Luna, G. P. Lopez and C. J. Brinker, *Nature*, 2000, **405**, 56; (*c*) B. Hatton, L. Mishchenko, S. Davis, K. H. Sandhage and J. Aizenberg, *Proc. Natl. Acad. Sci. U. S. A.*, 2010, **107**, 10354; (*d*) H.-J. Jeon, K. H. Kim, Y.-K. Baek, D. W. Kim and H.-T. Jung, *Nano Lett.*, 2010, **10**, 3604; (*e*) C. Y. Khripin, D. Pristinski, D. R. Dunphy, C. J. Brinker and B. Kaehr, *ACS Nano*, 2011, **5**, 1401.

5 (*a*) S. M. Holmes, B. E. Graniel-Garcia, P. Foran, P. Hill, E. P. L. Roberts, B. H. Sakakini and J. M. Newton, *Chem. Commun.*, 2006, 2662; (*b*) M. Perez-Cabero, V. Puchol, D. Beltran and P. Amoros, *Carbon*, 2008, **46**, 297.

6 (*a*) K. H. Sandhage and Z. Bao, *U.S. Patent 7,615,206*, November 10, 2009; (*b*) K. H. Sandhage, *U.S. Patent 7,067,104*, June 27, 2006; (*c*) K. H. Sandhage, M. B. Dickerson, P. M. Huseman, M. A. Caranna, J. D. Clifton, T. A. Bull, T. J. Heibel, W. R. Overton and M. E. A. Schoenwaelder, *Adv. Mater.*, 2002, **14**, 429; (*d*) Z. Bao, M. R. Weatherspoon, S. Shian, Y. Cai, P. D. Graham, S. M. Allan, G. Ahmad, M. B. Dickerson, B. C. Church, Z. Kang, H. W. Abernathy, C. J. Summers, M. Liu and K. H. Sandhage, *Nature*, 2007, **446**, 172; (*e*) Z. Bao, E. M. Ernst, S. Yoo and K. H. Sandhage, *Adv. Mater.*, 2009, **21**, 474.

7 Y. Gogotsi, S. Welz, D. A. Ersoy and M. J. McNallan, *Nature*, 2001, **411**, 283.

8 G. G. Tibbetts, G. L. Doll, D. W. Gorkiewicz, J. J. Moleski, T. A. Perry, C. J. Dasch and M. J. Balogh, *Carbon*, 1993, **31**, 1039.

9 J. Browning, P. L. Goggin, R. J. Goodfellow, M. G. Norton, A. J. M. Rattray, B. F. Taylor and J. Mink, *J. Chem. Soc., Dalton Trans.*, 1977, 2061.

10 Powder Diffraction File, Card No. 89-2955 for Si, Card No. 73-1708 for β-SiC, Card No. 75-0444 for C (International Center on Diffraction Data, Newtown Square, PA).

11 M. Iwaki, *Surf. Coat. Technol.*, 2002, **158–159**, 377.

12 A. L. Dicks, *J. Power Sources*, 2006, **156**, 128.

13 F. Barbir and S. Yazici, *Int. J. Energy Res.*, 2008, **32**, 369.


 